Dalton Transactions

COMMUNICATION

View Article Online
View Journal | View Issue

Cite this: *Dalton Trans.*, 2019, **48**, 1166

Received 10th September 2018,
Accepted 30th November 2018

DOI: 10.1039/c8dt03653e

rsc.li/dalton

A microstructured p-Si photocathode outcompetes Pt as a counter electrode to hematite in photoelectrochemical water splitting†

Anurag Kawde, [a,b] Alagappan Annamalai, [c] Anita Sellstedt,[d] Pieter Glatzel, [b] Thomas Wågberg[c] and Johannes Messinger *[a,e]

Herein, we communicate about an Earth-abundant semiconductor photocathode (p-Si/TiO_2/NiO_x) as an alternative for the rare and expensive Pt as a counter electrode for overall photoelectrochemical water splitting. The proposed photoelectrochemical (PEC) water-splitting device mimics the "Z"-scheme observed in natural photosynthesis by combining two photoelectrodes in a parallel-illumination mode. A nearly 60% increase in the photocurrent density (J_{ph}) for pristine α-Fe_2O_3 and a 77% increase in the applied bias photocurrent efficiency (ABPE) were achieved by replacing the conventionally used Pt cathode with an efficient, cost effective p-Si/TiO_2/NiO_x photocathode under parallel illumination. The resulting photocurrent density of 1.26 mA cm^{-2} at 1.23V_{RHE} represents a new record performance for hydrothermally grown pristine α-Fe_2O_3 nanorod photoanodes in combination with a photocathode, which opens the prospect for further improvement by doping α-Fe_2O_3 or by its decoration with co-catalysts. Electrochemical impedance spectroscopy measurements suggest that this significant performance increase is due to the enhancement of the space-charge field in α-Fe_2O_3.

Harvesting solar energy to split water into solar fuels such as hydrogen and oxygen by employing catalysts made of Earth-abundant elements is the crux of "artificial photosynthesis".[1–3] Hitherto, extensive research has been performed on designing photoelectrochemical (PEC) water-splitting devices and the respective photocathodes[4] and photoanodes.[5] Arranging the photoelectrodes in the parallel-illumination mode replicating the "Z"-scheme of natural photosynthesis[6] is one option for employing the abundant solar energy in an effective way.[7] The major challenges for designing Z-scheme devices include the positioning of the respective band edges so that the conduction band minimum of the photoanode lies at a lower electrochemical potential than the valence band maximum of the photocathode.[1,8] In addition, finding a favourable aqueous environment for both the photoelectrodes to achieve an efficient PEC performance for long time periods is difficult as most photoanodes are stable at alkaline pH, while the majority of the photocathodes work best at acidic pH.[9]

Recently, Jang *et al.*[10] have reported a tandem PEC device that comprised ZnO/a-Si/TiO_2/Pt as a photocathode and modified hematite (FTO/α-Fe_2O_3-$NiFeO_x$) as a photoanode. This Pt-containing device had a solar-to-hydrogen efficiency of 0.91% and thus demonstrated that combining Si and hematite in a tandem device is a promising approach. Tandem PEC devices[10–14] require a semi/transparent front photoelectrode (photoanode) with a wide bandgap energy and a rear photocathode with a narrow band gap energy. Thus, tandem PEC configurations are associated with strict fabrication constraints.[15] On the other hand, the parallel-illumination mode selected in the present study gives the freedom to use opaque photoelectrodes for simultaneous illumination, adding considerable extra flexibility in the device design. We report here a Pt-free device that combines a well-studied pristine α-Fe_2O_3 photoanode[16,17] in aqueous 1 M NaOH (pH 13.8; best conditions for α-Fe_2O_3) with a previously optimized micro-structured p-Si/TiO_2/NiO_x photocathode.[18] We demonstrate that this Z-scheme device outcompetes a similar device featuring a Pt cathode. This approach has excellent potential for future optimization since the Earth-abundant Si and Fe_2O_3 photoelectrodes have thermodynamic solar-to-hydrogen conversion capabilities of ~43% and ~15%, respectively.[19]

The PEC performance of the pristine α-Fe_2O_3 photoanode was measured (see the ESI† for experimental details) against either a Pt or a microstructured p-Si cathode that was protected by a spin-coated TiO_2 layer and functionalized with a Ni-oxide catalyst (p-Si/TiO_2/NiO_x).[18] These single (α-Fe_2O_3) illumination

[a]*Umeå University, Department of Chemistry, Sweden. E-mail: johannes.messinger@kemi.uu.se*
[b]*European Synchrotron Radiation Facility (ESRF), Grenoble, France*
[c]*Umea University, Department of Physics, Sweden*
[d]*Umeå University, Department of Plant Physiology, Umeå Plant Science Centre (UPSC), Umeå, Sweden*
[e]*Molecular Biomimetics, Department of Chemistry, Ångström Laboratory, Uppsala University, Sweden*

†Electronic supplementary information (ESI) available. See DOI: 10.1039/c8dt03653e

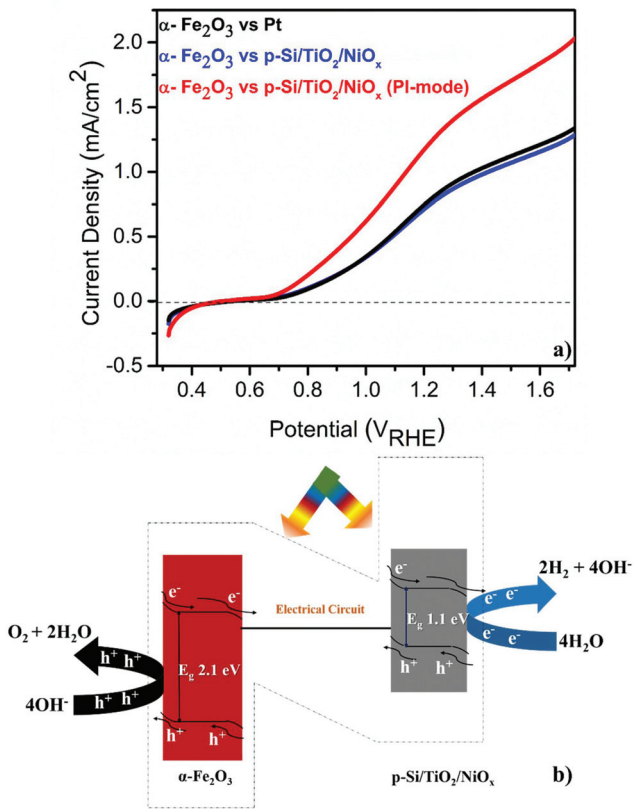

Fig. 1 (a) Linear sweep voltammograms of a pristine α-Fe_2O_3 photoanode *vs.* Pt or p-Si/TiO_2/NiO_x in 1 M NaOH (pH 13.8) under standard (1 sun) single or parallel illumination (PI-mode). (b) Schematic band diagram illustrating Z-scheme overall water splitting.

configurations are compared to a Z-scheme configuration, in which the p-Si/TiO_2/NiO_x electrode was also illuminated at 1 sun and acted as a photocathode (Fig. 1a and b). The detailed and systematic half-cell characterization studies of both photoelectrodes have been presented recently.[16–18] In agreement with these earlier studies, Fig. 1a shows that pristine α-Fe_2O_3 oxidizes, in conjunction with a Pt counter electrode, water with a photocurrent density (J_{ph}) of 0.80 mA cm^{-2} in 1 M NaOH (pH 13.8) and 1.23V_{RHE}. Consistent with the expectation that the hole diffusion length in the pristine α-Fe_2O_3 photoanode limits the overall PEC performance, we found that J_{ph} barely changed (0.77 mA cm^{-2}) when p-Si/TiO_2/NiO_x was used instead of Pt and only α-Fe_2O_3 was illuminated. Remarkably, an unprecedented increase in J_{ph} to 1.26 mA cm^{-2} was recorded when both α-Fe_2O_3 and p-Si/TiO_2/NiO_x were illuminated simultaneously in the parallel-illumination mode (see the photograph of the PEC cell; Fig. S1†). The elemental and morphological characterization results of the photoelectrodes are shown in Fig. S2 and S3.† Z-scheme illumination is thus an efficient complementary approach for boosting the efficiency of the PEC performance of pristine α-Fe_2O_3. Previous studies have shown performance enhancements of up to ~100% by introducing different dopants[5,20–22] or suitable underlayers[23–25] (see Table S1† with the PEC performance of functionalized α-Fe_2O_3 and different electrode assemblies under different illumination conditions). The proposed band energy schematic for overall Z-scheme water splitting is shown in Fig. 1b.[1,8] As detailed below, the observed significant increase in the J_{ph} (~60%) in this configuration may be attribu-

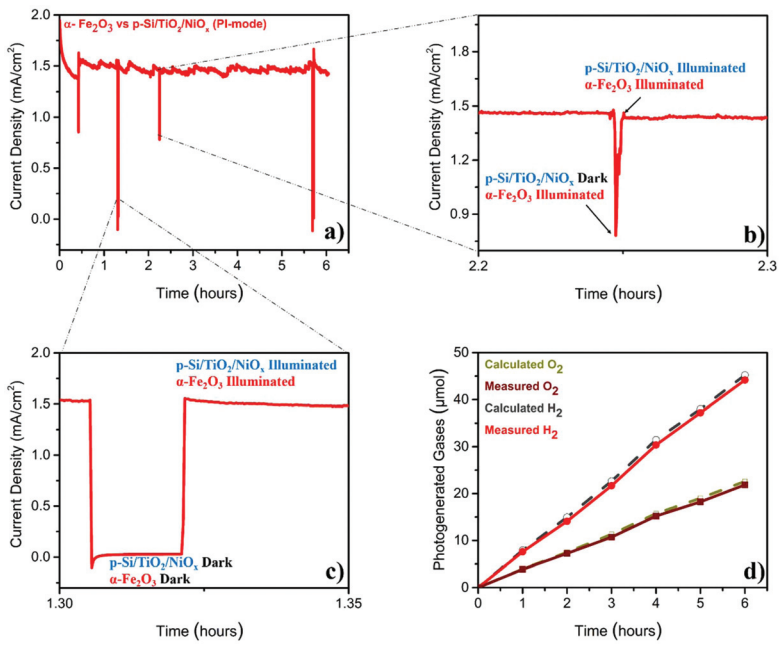

Fig. 2 Photo-electrochemical characterization of α-Fe_2O_3 *vs.* p-Si/TiO_2/NiO_x in 1 M NaOH (pH 13.8) under standard (1 sun) parallel illumination mode (PI-mode) (a) photocurrent density measured at 1.4V_{RHE}; (b) magnified section showing the photocurrent when only α-Fe_2O_3 is illuminated; (c) magnified section showing the dark current; (d) comparison of calculated and measured photo-generated hydrogen and oxygen (illuminated area of α-Fe_2O_3 was 0.09 cm^2 and that of p-Si/TiO_2/NiO_x was 0.18 cm^2).

ted to the enhanced generation of minority carriers at the p-Si/TiO_2/NiO_x photocathode, leading to an increased hole-utilization for water oxidation at the surface of the α-Fe_2O_3 photoanode.

The stability test (Fig. 2a), performed at $1.4V_{RHE}$, demonstrated that the Z-scheme setup operated, after a slight decay in the first 30 min, at a stable photocurrent density of ~1.5 mA cm^{-2} over the entire six-hour experiment. The sharp 'spikes' in Fig. 2a were produced by blocking the illumination of the p-Si/TiO_2/NiO_x electrode (Fig. 2b), or of both electrodes (Fig. 2c), demonstrating the photocurrent effects. The gases generated during this parallel-illumination PEC water-splitting experiment were collected and quantified using gas chromatography. The data in Fig. 2d show a stable and stoichiometric light-driven generation of O_2 and H_2, amounting to ~158 μmol cm^{-2} H_2 and ~78 μmol cm^{-2} O_2, which corresponded to a faradaic efficiency of ~96% (the illuminated area of α-Fe_2O_3 was 0.09 cm^2 and that of p-Si/TiO_2/NiO_x was 0.18 cm^2). We additionally examined the photoelectrodes before and after the 6-hour PEC experiment employing X-ray spectroscopy. These high-energy resolution fluorescence detected X-ray absorption near edge structure (HERFD-XANES) and X-ray emission spectroscopy (XES) experiments did not reveal any indications for changes of the photoelectrodes (ESI Fig. S4†).

Given this excellent stability, we determined the applied bias photocurrent efficiencies (ABPE) (Fig. 3(a)), the flat band potentials (V_{fb}) (Fig. 3(b)) and the onset potentials (V_{onset}) (Fig. 3(c)). In the parallel-illumination mode, a maximum ABPE of ~0.14% was obtained, which is, taking the absorption of additional photons by the p-Si/TiO_2/NiO_x photocathode into account, ~77% higher than that obtained with Pt as the counter electrode. Furthermore, V_{fb} and V_{onset} potentials deduced in the parallel-illumination mode were 100 mV and 40 mV lower as compared to using a Pt counter electrode. These remarkable results further substantiate the idea that the extra holes provided by the p-Si/TiO_2/NiO_x photocathode increased the hole flux towards water oxidation by enhancing the space-charge region in the α-Fe_2O_3 photoanode.[13,26,27] Our observation is in agreement with earlier studies,[28–31] wherein a large enough space-charge region (increased space-charge field) leads to the generation of relatively "long-lived" photogenerated holes that accumulate at the α-Fe_2O_3 electrode surface resulting in increased O_2 evolution.

To test this idea, electrochemical impedance spectroscopy (EIS) was performed. As shown in Fig. 4, replacing the Pt counter electrode by the p-Si/TiO_2/NiO_x photocathode improved the interfacial charge-transfer kinetics significantly. The charge-transfer resistance (R_{CT2} – larger semicircular region) across the photoanode/electrolyte interface reduced from 439.8 Ω to 298.2 Ω. The 33% decrease in R_{CT2} is attributed to the favorable band edge shifts in both α-Fe_2O_3 and p-Si/TiO_2/NiO_x under parallel illumination leading to a more effective transfer of photoexcited charge carriers to the surface of the respective photoelectrodes. These effective band edge shifts also increased the surface charges of the α-Fe_2O_3 photoanode, thereby allowing for a better surface adsorption of OH^- onto α-Fe_2O_3, which improved the charge-transfer kinetics at the photoanode/electrolyte interface. However, the Z-scheme configuration also led to an undesired increase in hole recombination losses in the bulk of the α-Fe_2O_3 photoanode, as wit-

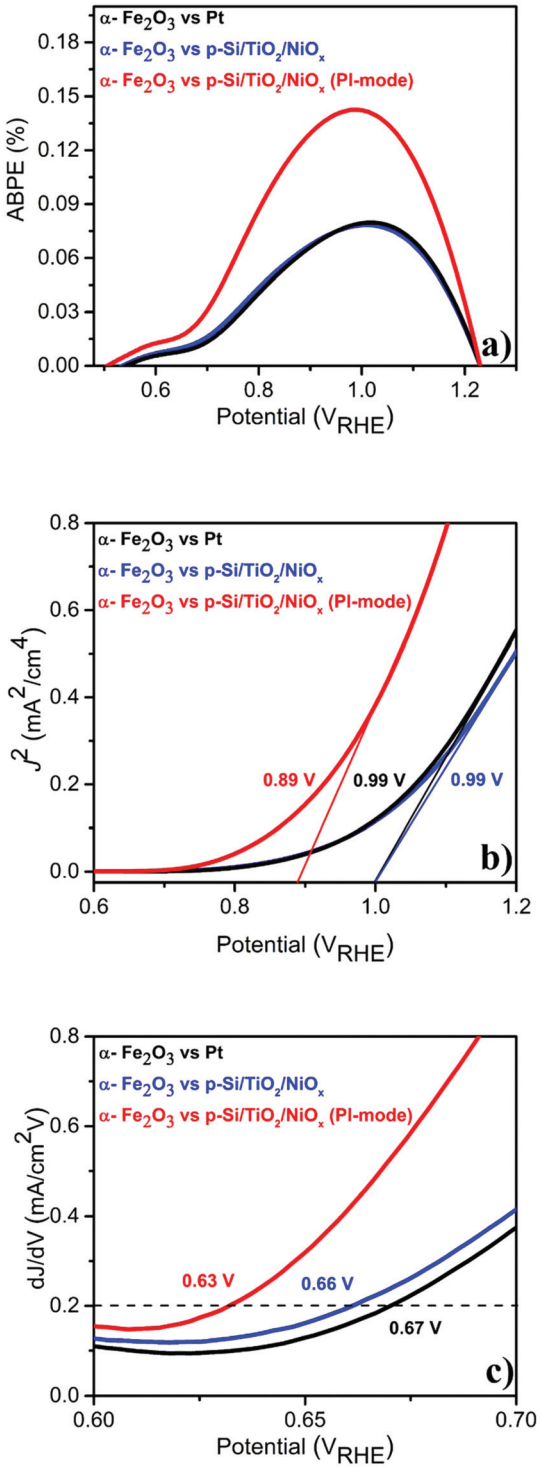

Fig. 3 Photo-electrochemical performance of α-Fe_2O_3 *vs.* Pt or p-Si/TiO_2/NiO_x in 1 M NaOH (pH 13.8) under standard (1 sun) single or parallel illumination (PI-mode) derived from LSVs shown in Fig. 1 (a) ABPE (%) (b) flat-band potential (V_{fb}) and (c) V_{onset}.

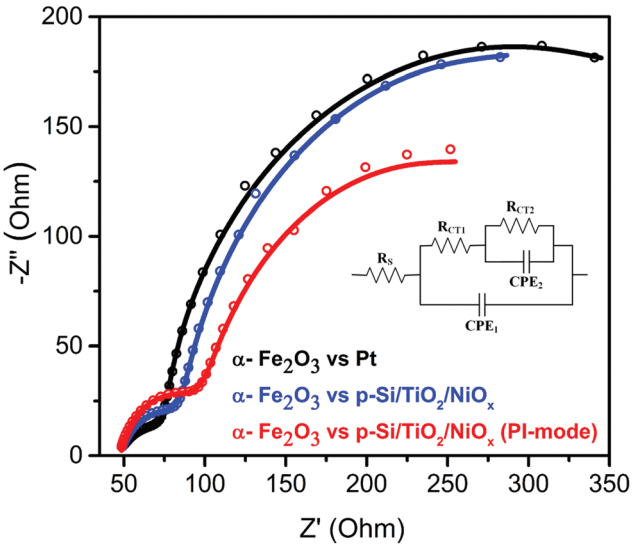

Fig. 4 Nyquist plots of α-Fe_2O_3 *vs.* Pt or p-Si/TiO_2/NiO_x in 1 M NaOH (pH 13.8) under standard (1 sun) single or parallel illumination (PI-mode). The inset shows the equivalent circuit[30] employed for analyzing the Nyquist plots. The fit data are provided in ESI Table S2.†

nessed by the increased intrinsic charge-transfer resistance (R_{CT1} – smaller semicircular region) from 42.09 to 64.26 Ω. This suggests that the sluggish hole mobility in the hematite photoanodes and the resulting recombination losses remained a bottleneck for the overall performance, in agreement with several previous studies.[5,27,32] However, such losses may be minimized in the future by using suitable dopants for α-Fe_2O_3.[20,33,34]

Our results demonstrate that aqueous NaOH (pH 13.8) is a favorable environment for both the α-Fe_2O_3 photoanode and the p-Si/TiO_2/NiO_x photocathode, allowing stable Z-scheme device operation for overall light-driven water splitting with significantly better performance as compared to Pt counter electrodes.

Conclusions

A noteworthy photocurrent density (J_{ph}) of 1.26 mA cm^{-2} at 1.23V_{RHE} was achieved using a pristine α-Fe_2O_3 photoanode in combination with a micro-structured p-Si/TiO_2/NiO_x photocathode in parallel illumination, clearly outcompeting conventional device designs employing Pt counter electrodes. The micro-structured p-Si/TiO_2/NiO_x photocathode in this Z-scheme configuration improved the charge-transfer kinetics at the α-Fe_2O_3 photoanode/electrolyte interface, but also led to increased bulk recombination. This suggests that this Z-scheme device can be readily improved in future by suitable doping of the α-Fe_2O_3 photoanode and by functionalization with catalysts.

Conflicts of interest

The authors declare no competing financial interest.

Acknowledgements

The authors thank the European Synchrotron Radiation Facility for granting beamtime and the ID 26 beamline staff for the assistance during the experiments. The Knut and Alice Wallenbergs Foundation (Artificial Leaf Project; KAW 2011.0055) provided financial support. T. W. acknowledges support from Vetenskapsrådet (2017-04862), Energimyndigheten (45419-1), and Ångpanneföreningen (15-483).

References

1 M. Grätzel, *Nature*, 2001, **414**, 338.
2 M. G. Walter, E. L. Warren, J. R. McKone, S. W. Boettcher, Q. Mi, E. A. Santori and N. S. Lewis, *Chem. Rev.*, 2010, **110**, 6446–6473.
3 Y. Tachibana, L. Vayssieres and J. R. Durrant, *Nat. Photonics*, 2012, **6**, 511.
4 Y. Hou, B. L. Abrams, P. C. Vesborg, M. E. Björketun, K. Herbst, L. Bech, A. M. Setti, C. D. Damsgaard, T. Pedersen and O. Hansen, *Nat. Mater.*, 2011, **10**, 434.
5 A. Kay, I. Cesar and M. Grätzel, *J. Am. Chem. Soc.*, 2006, **128**, 15714–15721.
6 W. Lubitz, E. J. Reijerse and J. Messinger, *Energy Environ. Sci.*, 2008, **1**, 15–31.
7 S. Ida, K. Yamada, T. Matsunaga, H. Hagiwara, Y. Matsumoto and T. Ishihara, *J. Am. Chem. Soc.*, 2010, **132**, 17343–17345.
8 N. Queyriaux, N. Kaeffer, A. Morozan, M. Chavarot-Kerlidou and V. Artero, *J. Photochem. Photobiol., C*, 2015, **25**, 90–105.
9 S. Chen and L.-W. Wang, *Chem. Mater.*, 2012, **24**, 3659–3666.
10 J.-W. Jang, C. Du, Y. Ye, Y. Lin, X. Yao, J. Thorne, E. Liu, G. McMahon, J. Zhu and A. Javey, *Nat. Commun.*, 2015, **6**, 7447.
11 Y. Qiu, W. Liu, W. Chen, G. Zhou, P.-C. Hsu, R. Zhang, Z. Liang, S. Fan, Y. Zhang and Y. Cui, *Sci. Adv.*, 2016, **2**, e1501764.
12 J. Luo, J.-H. Im, M. T. Mayer, M. Schreier, M. K. Nazeeruddin, N.-G. Park, S. D. Tilley, H. J. Fan and M. Grätzel, *Science*, 2014, **345**, 1593–1596.
13 C. Ding, W. Qin, N. Wang, G. Liu, Z. Wang, P. Yan, J. Shi and C. Li, *Phys. Chem. Chem. Phys.*, 2014, **16**, 15608–15614.
14 L. Pan, J. H. Kim, M. T. Mayer, M.-K. Son, A. Ummadisingu, J. S. Lee, A. Hagfeldt, J. Luo and M. Grätzel, *Nat. Catal.*, 2018, **1**, 412.
15 Y. Kuang, T. Yamada and K. Domen, *Joule*, 2017, **1**(2), 290–305.
16 A. Annamalai, A. Subramanian, U. Kang, H. Park, S. H. Choi and J. S. Jang, *J. Phys. Chem. C*, 2015, **119**, 3810–3817.
17 A. Annamalai, P. S. Shinde, T. H. Jeon, H. H. Lee, H. G. Kim, W. Choi and J. S. Jang, *Sol. Energy Mater. Sol. Cells*, 2016, **144**, 247–255.
18 A. Kawde, A. Annamalai, L. Amidani, M. Boniolo, W. L. Kwong, A. Sellstedt, P. Glatzel, T. Wagberg and J. Messinger, *Sustainable Energy Fuels*, 2018, **2**, 2215–2223.

19 Z. Chen, T. F. Jaramillo, T. G. Deutsch, A. Kleiman-Shwarsctein, A. J. Forman, N. Gaillard, R. Garland, K. Takanabe, C. Heske and M. Sunkara, *J. Mater. Res.*, 2010, **25**, 3–16.
20 A. Annamalai, R. Sandström, E. Gracia-Espino, N. Boulanger, J.-F. Boily, I. Mühlbacher, A. Shchukarev and T. Wågberg, *ACS Appl. Mater. Interfaces*, 2018, **10**, 16467–16473.
21 A. Y. Ahmed, M. G. Ahmed and T. A. Kandiel, *J. Phys. Chem. C*, 2016, **120**, 23415–23420.
22 A. Kay, D. A. Grave, D. S. Ellis, H. Dotan and A. Rothschild, *ACS Energy Lett.*, 2016, **1**, 827–833.
23 K. Sivula, F. L. Formal and M. Gratzel, *Chem. Mater.*, 2009, **21**, 2862–2867.
24 A. Annamalai, P. S. Shinde, A. Subramanian, J. Y. Kim, J. H. Kim, S. H. Choi, J. S. Lee and J. S. Jang, *J. Mater. Chem. A*, 2015, **3**, 5007–5013.
25 I. S. Cho, H. S. Han, M. Logar, J. Park and X. Zheng, *Adv. Energy Mater.*, 2016, **6**, 1501840.
26 J. Brillet, J.-H. Yum, M. Cornuz, T. Hisatomi, R. Solarska, J. Augustynski, M. Graetzel and K. Sivula, *Nat. Photonics*, 2012, **6**, 824.
27 P. S. Shinde, S. H. Choi, Y. Kim, J. Ryu and J. S. Jang, *Phys. Chem. Chem. Phys.*, 2016, **18**, 2495–2509.
28 D. A. Wheeler, G. Wang, Y. Ling, Y. Li and J. Z. Zhang, *Energy Environ. Sci.*, 2012, **5**, 6682–6702.
29 F. Le Formal, S. R. Pendlebury, M. Cornuz, S. D. Tilley, M. Grätzel and J. R. Durrant, *J. Am. Chem. Soc.*, 2014, **136**, 2564–2574.
30 T. Lopes, L. Andrade, F. Le Formal, M. Gratzel, K. Sivula and A. Mendes, *Phys. Chem. Chem. Phys.*, 2014, **16**, 16515–16523.
31 F. Le Formal, E. Pastor, S. D. Tilley, C. A. Mesa, S. R. Pendlebury, M. Grätzel and J. R. Durrant, *J. Am. Chem. Soc.*, 2015, **137**, 6629–6637.
32 L. Jia, K. Harbauer, P. Bogdanoff, I. Herrmann-Geppert, A. Ramírez, R. van de Krol and S. Fiechter, *J. Mater. Chem. A*, 2014, **2**, 20196–20202.
33 W. L. Kwong, C. C. Lee, A. Shchukarev, E. Björn and J. Messinger, *J. Catal.*, 2018, **365**, 29–35.
34 R. Zhang, Y. Fang, T. Chen, F. Qu, Z. Liu, G. Du, A. M. Asiri, T. Gao and X. Sun, *ACS Sustainable Chem. Eng.*, 2017, **5**, 7502–7506.